



**HAL**  
open science

## Control of a Robot Axis with Effort Feedback

Sofia Torres, Pierre-Philippe Robet, Yannick Aoustin, Maxime Gautier, Jorge Martins

► **To cite this version:**

Sofia Torres, Pierre-Philippe Robet, Yannick Aoustin, Maxime Gautier, Jorge Martins. Control of a Robot Axis with Effort Feedback. MIM2022, IFAC (International federation of automatic control, Jun 2022, Nantes, France. hal-03718821

**HAL Id: hal-03718821**

**<https://hal.science/hal-03718821>**

Submitted on 9 Jul 2022

**HAL** is a multi-disciplinary open access archive for the deposit and dissemination of scientific research documents, whether they are published or not. The documents may come from teaching and research institutions in France or abroad, or from public or private research centers.

L'archive ouverte pluridisciplinaire **HAL**, est destinée au dépôt et à la diffusion de documents scientifiques de niveau recherche, publiés ou non, émanant des établissements d'enseignement et de recherche français ou étrangers, des laboratoires publics ou privés.

# Control of a Robot Axis with Effort Feedback

Sofia Torres\*\* Pierre-Philippe Robet\* Yannick Aoustin\*  
Maxime Gautier\* Jorge Martins\*\*

\* Nantes Université, LS2N (Laboratoire des Sciences du Numérique de Nantes), UMR CNRS 6004, Nantes, 44300 France (e-mail: (Pierre-philippe.Robet, Yannick.Aoustin, Maxime.Gautier)@univ-nantes.fr).

\*\* IDMEC, Instituto Superior Técnico, Universidade de Lisboa, Lisboa, Portugal (e-mail: jorgemartins@tecnico.ulisboa.pt)

---

**Abstract:** This paper tackles the control design of a robot to handle said interaction. A new model is written of an EMPS Prototype to emulate a robot-environment scenario, including now two masses and with their interaction translated as a spring and damper system, followed by the implementation of a cascaded loop of force-velocity control of the robot axis. A new formulation of the force control is also designed and implemented considering the impedance control theory. Finally, this model and its cascaded loop control is validated against real values through the experiment proving its accuracy.

*Keywords:* control, robotics, impedance, experimental validation

---

## 1. INTRODUCTION

The world of robotics has evolved through multiple fields since Isaac Asimov formulated the Three Laws of Robotics in 1942 and coined the word "robotics". Depending on which task the robot has to deal with, environment interaction can be a big issue or not. For example, the KUKA robot can be used for welding in the automotive industry, where it is taught a specific trajectory and velocity profile, since its environment is unchanged throughout time. Since its interaction with its environment is already predefined, the robot-environment question is not necessarily an issue. In the robotic-surgery field, the DLR-MIRO is an example of a robot system designed to "assist a surgeon directly at the operating table where space is scarce". In this case, its environment is not necessarily straightforward and cannot be fully defined prior to its interaction, creating a new questions to its designers, like: *How can we control the robot to perform a specified task? How will the environment respond? Or how can we control said response?*

When the environment response comes into play, it will depend immensely on the system's surroundings. A stiff object can be easily thought as a spring with a high value, in the other hand a soft tissue interaction can be very unpredictable. How we control a robot-environment response can be through hybrid force/velocity control when the case is well structured and geometrically defined environments. In this case, with a structured environment, force profiles are easily designed as reference for the robot to follow, but if the environment is unstructured and dynamically changing, impedance control will be more adequate, where we define the kind of dynamic response we desire from the interaction robot-environment instead of a specific force profile.

Impedance control has now been the focus of research in works like Albu-Schaffer et al. (2007), Albu-Schaffer et al. (2003), Albu-Schaffer and Hirzinger (2002), where light-weight robots are the focus and torque-feedback controllers as well as impedance schemes are implemented and tested. In the work of Devie et al. (2017) and Devie et al. (2018), the robot in question is a one-axis system with a force sensor. So far a cascaded force-velocity control loop has been designed to answer question number 1 and also some strides have been made to answer question 3 through the force control but also with an impedance control, like the one described in Devie et al. (2018), where an effort was made to compare these two types of control and it was concluded that they were equivalent.

The goal of this paper is to extend the research of Devie et al. (2017) and Devie et al. (2018). While so far the design of controllers has been made on the assumption that the two mass model can be simplified into a one mass model, this assumption has not been fully analyzed or validated with the real system, in sec. 2 a new model is formulated and in sec. 3 its validation is performed. Section 4 offers our conclusion and perspectives.

## 2. A SYSTEM OF TWO MASSES: MODEL AND CONTROL

The proposed system in fig. 1 intends to model the EMPS robot in a more complete manner than what was done so far, in particular the mass  $m$  and the viscous friction coefficient  $f_{v2}$  are considered.

### 2.1 System Modelling

The system consists of two masses  $M$  and  $m$ , which are connected by a spring with stiffness  $K$  and a damper

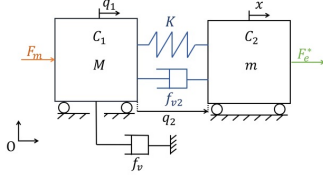


Fig. 1. Two Mass System - Schematic.

with a viscous friction coefficient  $f_{v2}$ , the mass  $M$  is also affected by a damper of viscous friction with coefficient  $f_v$  Yi et al. (2010), Zhang et al. (2016). The system moves in the horizontal direction and consists of two  $DoF$ , each connected to each mass, fig. 2. The position of the Mass  $M$  is described by  $q_1$  and the position of the mass  $m$  is described by  $x = q_1 + q_2$ . There are also two others inputs the motor force  $F_m$  applied to mass  $M$  and the environment contact force  $F_e^*$  applied to mass  $m$ . With this description the set of equations describing the full system's dynamics are:

$$\begin{cases} M\ddot{q}_1 = F_m - f_v\dot{q}_1 + Kq_2 + f_{v2}\dot{q}_2 \\ m\ddot{q}_2 = F_e^* - m\dot{q}_1 - Kq_2 - f_{v2}\dot{q}_2. \end{cases} \quad (1)$$

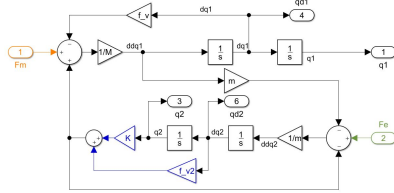


Fig. 2. Block diagram of the mechanical system.

## 2.2 Sensitivity Analysis

This system formulation adds two parameters: the mass  $m$  and the viscous friction coefficient  $f_{v2}$ . A sensibility analysis was done to understand the range of the parameters' values where the model still corresponds to the reality it is trying to simulate.

**Mass  $m$**  As it was previously mentioned, the mass  $m$  in our system was neglected in previous work. Table 1 we define a set of mass values, which will be used for a sensitivity analysis, where will make use of the Bode Diagrams to compare the resulting dynamics. The purpose will be to conclude what is the maximum value this mass element can have for the assumption made in previous work to hold. It is also important to notice the simulations were performed setting  $f_{v2} = 0\text{Ns/m}$ , thus ignoring the existence of this viscous element.

In the analysis it was considered only the input  $F_m$  and the position outputs  $q_1$  seen in fig. 3(a), and  $q_2$  seen in fig. 3(b). Since the range of values of  $q_2$  are several times lower than those of  $q_1$ , especially in haptic applications, this means that the dynamic response of  $x$  is very similar to  $q_1$ . For the same reason it will make more sense to only analyse the Bode Diagram of  $q_2$  and not of  $x$ .

The mass  $m$  has a clear influence in the natural frequency of the system. This frequency is calculated, considering the motion of the center of mass of the two-mass system, which leads to the following equations:

$$M_{eq} = \frac{1}{\frac{1}{M} + \frac{1}{m}} = \frac{Mm}{M+m} \quad (2)$$

$$\omega_n = \sqrt{\frac{K}{M_{eq}}} = \sqrt{\frac{K(M+m)}{Mm}} \quad (3)$$

Table 1 has the values of mass  $m$  and the correspondent natural frequency. In the obtained results we see that for a mass  $m$  up to 10kG the dynamic behavior of  $q_1$  is maintained while the natural frequency, where the peaks of magnitude happens, is moving according to the values in table 1. However, if we consider values above 10kG, the response in frequency domain deviates from the almost linear evolution in magnitude, especially for lower frequencies (below 100rad/s), *i.e.* the effect of mass  $m$  on the overall dynamics can no longer be ignored.

Table 1. Natural Frequency Values

$m$ [kg]	$\omega_n$ [rad/s]
0,1	447.44
1	142.16
10	47.01
100	20.26
1000	15.18

**Friction Coefficient  $f_{v2}$**  Considering now the friction coefficient  $f_{v2}$  connecting the two masses, we will focus on the dynamic behavior of mass  $m$ , where we set  $m = 0.1\text{kg}$ . The natural frequency just considering a stiffness  $K$  and mass  $m$  is  $\omega_{n2} = \sqrt{\frac{K}{m}} = 447.2\text{rad/s}$  and the respective time period of a step response is  $T_p = \frac{2\pi}{\omega_{n2}} = 0.014\text{s}$ . The time period can be checked in time response to a step input with  $F_e^* = 10\text{N}$  in fig. 4(b), as well as the steady state value of the final position where we have  $q_2 = F_e^*/K = 0.0005\text{m}$ .

Considering the different values of  $f_{v2}$  in fig. 4(a), we see

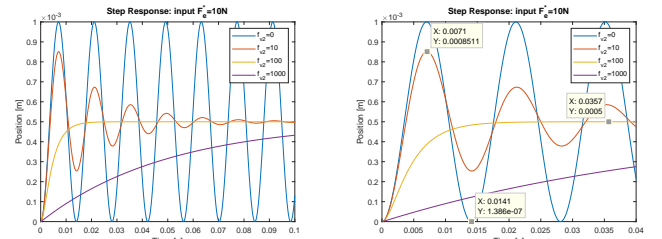


Fig. 4. Friction Influence: Step Response from an  $F_e^*$  input.

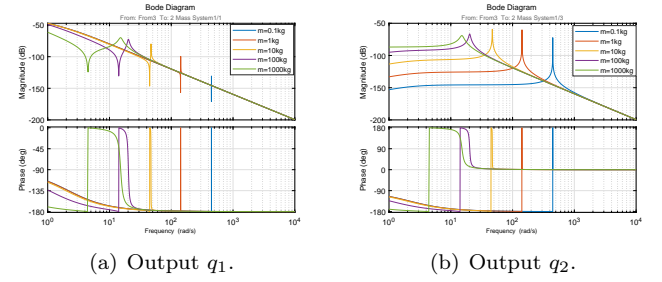


Fig. 3. Mass Influence: Bode Diagram for an  $F_m$  input.

an underdamped system for values 0 and 10Ns/m with oscillatory responses, for  $f_{v2} = 100\text{Ns/m}$  we see a critically damped system with no overshoot and a fast settling time of  $T_s = 0.015\text{s}$ , a desired response, and finally with a value of  $1000\text{Ns/m}$  the system has an overdamped response with a very slow time response of  $T_s = 0.2\text{s}$ .

A last analysis was done with the complete model and its Bode Diagram was analyzed (figs 5(a) and 5(b)). For the dynamic of  $q_1$  the resonance disappears for friction values different than zero, but otherwise the frequency response maintains constant. While considering the dynamic of  $q_2$  for values below  $100\text{Ns/m}$  it has a peak value in magnitude for the natural frequency that does not occur for a  $100\text{Ns/m}$  of friction coefficient - the critically damped case. When considering a full model for future simulations

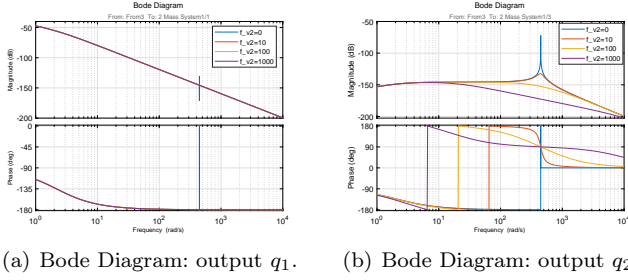


Fig. 5. Friction Influence: input  $F_m$ .

a friction coefficient value of  $100\text{Ns/m}$  will be used, because of its critically damped behavior that gives the fastest response possible without overshoot. A final and true value can only be obtained with the experimental validation.

### 2.3 Velocity Control Loop

**Control Design** To implement a closed loop control of the velocity  $\dot{q}_1$  like the one in Devie et al. (2017), it was first considered a simplified model with  $m = 0\text{kG}$ . This means that the system consists only of a mass  $M$  and a damper of coefficient  $f_v$ , with the transfer function

$$T_M = \frac{\dot{q}_1}{F_m} = \frac{1}{Ms + f_v}. \quad (4)$$

The controller considered is an Integral and Proportional (IP) controller, obtaining a fast response with a lower overshoot when compared to a PI controller. The open loop transfer function considering the velocity controller and the mass-damper system is written in (5). This transfer function is then used to calculate the control gains.

$$T_v = \frac{\dot{q}_1}{\dot{q}_{ref} - \dot{q}_1} = \frac{k_v G_\tau}{t_v s} \frac{1}{Ms + f_v + k_v G_\tau} \quad (5)$$

We want  $T_v(j\omega_v) = 1e^{j(-\pi+\phi_v)}$ , with frequency  $\omega_v = 200\text{rad/s}$  and a phase margin  $\phi_v$  of  $70^\circ$ . We obtain the expressions for the controller gains  $k_v$  and  $t_v$  in (6) and (7) respectively.

$$k_v = \frac{M\omega_v \tan(\phi_v) - f_v}{G_\tau} = 1.4856 \cdot 10^3 \quad (6)$$

$$t_v = \frac{k_v G_\tau}{M\omega_v^2} \cos(\phi_v) = 0.0047 \quad (7)$$

With the set of controller gains calculated, the control scheme is added to the full two mass model and the Bode

Diagram from input  $\dot{q}_{ref}$  to outputs  $\dot{q}_1$  and  $\dot{x}$  is evaluated, Fig. 6. Firstly, we see that  $\dot{q}_1$  and  $\dot{x}$  have the same dynamic

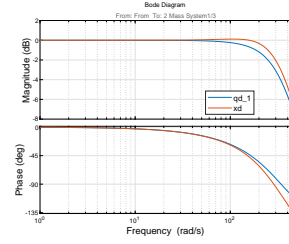


Fig. 6. Velocity Control-Bode Diagram comparison between the two outputs:  $\dot{q}_1$  and  $\dot{x}$

response which is to follow the desired velocity input, at a frequency  $100\text{rad/s}$  their magnitude starts to decrease, *i.e.* the input desired velocity starts to no longer have an effect on their response. Finally, up until a frequency  $100\text{rad/s}$  the dynamic response of both outputs are equal or up to a difference of  $0.4\text{dB}$  (a negligible difference).

**Sensitivity Analysis** It is important to understand how the inner control loop changes the system, therefore a sensitivity analysis will be performed to evaluate the influence of the parameters in the new system.

**2.3.2.1. Mass m** For values of  $m \{0.1, 10, 1000\}\text{kG}$  the dynamic of  $\dot{q}_1$  in fig. 7(a) is not affected by an increase of mass, as the difference of magnitude between the systems corresponding to each of the three masses is around  $0.4\text{dB}$  maximum, happening only at the natural frequency. While the response of  $\dot{x}$  in fig. 7(b) is clearly affected with values above  $10\text{kG}$  inclusive, where the magnitude peaks at the natural frequency values and the system could become unstable, furthermore the phase of  $\dot{x}$  goes to  $-180^\circ$  much earlier for higher mass values, *i.e.* mass  $m$  will be moving in opposite direction with respect to mass  $M$ , which is highly undesirable. Only for values of mass below  $10\text{kG}$  the difference between  $\dot{q}_1$  and  $\dot{x}$  is negligible, within the working frequency range.

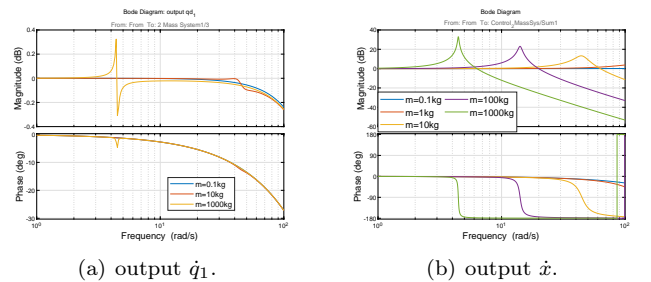


Fig. 7. Velocity Control - Bode Diagram comparison between the two outputs:  $\dot{q}_1$  and  $\dot{x}$ .

**2.3.2.2. Friction Coefficient  $f_{v2}$**  The influence of the damping system in the dynamics of  $\dot{q}_1$  except for the natural frequency with  $f_{v2} = 0$ . While considering the dynamics of  $\dot{x}$ , the impact of the damping system is more evident, as increasing the friction value up to  $100\text{Ns/m}$

decreases the peak magnitude value. Furthermore the responses are very similar up to 1000rad/s for systems with a friction coefficient between 100 and 1000Ns/m. With this analysis we can say that for lower values of  $f_{v2}$ , mass  $m$  will start oscillating earlier and with a higher magnitude, *i.e.* can become an unstable system. On the other side, for higher values of  $f_{v2}$ , mass  $m$  has a more compliant response, *i.e.* for the working frequency range mass  $m$  follows the dynamic response of  $M$ .

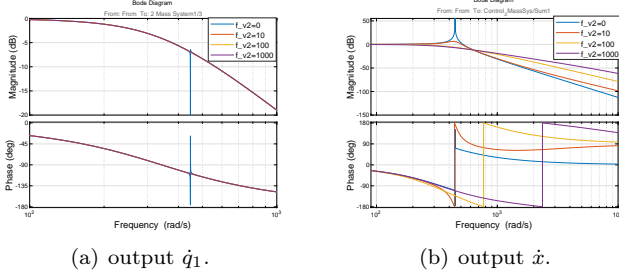


Fig. 8. Velocity Control - Friction Coefficient Influence: Bode Diagram.

## 2.4 Force Controller

**Control Design** A proportional force control was designed as the outer loop of the cascade control. In this type of control the most critical configuration while interacting with the environment is when it encounters a rigid obstacle with a stiffness that tends to infinity, this means that the equivalent stiffness of the set: Sensor + Environment, is equal to the stiffness  $K$ . It also means that the position of the end-effector is constant at  $x = 0$ . To achieve this we set  $q_1 = -q_2$  and we can write the value measured by the force sensor as  $-F_e = Kq_1 = K\frac{\dot{q}_1}{s}$  with  $f_{v2}$  neglected. With these assumptions we can obtain an expression for the force control gain  $k_e$ .

To obtain the control gain, we first need to write the closed loop transfer function of the velocity control and then it is straightforward to close the outer loop with the proportional force control, as seen in (8), and compute the frequency  $\omega_e$  through (9), considering a desired phase margin of  $\phi_e = 70^\circ$ .

$$T_f = \frac{-F_e}{F_{ref} - F_e} = T_{vclosed} k_e \frac{K}{s} \quad (8)$$

$$\omega_e = \omega_{0v}(-z_v \tan(\phi_e) + \sqrt{1 + \tan^2(\phi_e) z_v^2}) = 73.8531 \text{ rad/s} \quad (9)$$

After calculating the frequency  $\omega_e$ , we are able to calculate the control gain  $k_e$  considering that we would like the following expression to be true  $|T_f(j\omega_e)| = 1$ , obtaining:

$$k_e = \frac{\omega_e}{K} \sqrt{\left(1 - \left(\frac{\omega_e}{\omega_{0v}}\right)^2\right)^2 + \left(2z_v \frac{\omega_e}{\omega_{0v}}\right)^2} = 0.0101 \quad (10)$$

**Simulation implementation** With the controller gains calculated, the control scheme is implemented with Matlab. It is worth noticing that to obtain the force sensor

value, we take the value of  $q_2$  and multiply it by the sensor's stiffness  $K$ , neglecting its viscous friction.

Afterwards we compare the dynamic response of  $Kq_1$  and  $Kx$ . The Bode Diagram shows that up until a frequency of 100rad/s they have equivalent performances, both masses moving as one body. For higher frequencies we see the peak magnitude still happening at the natural frequency  $f = 447 \text{ rad/s}$ , with  $Kq_1$ 's peak of magnitude happening much more abruptly due to the velocity control but rapidly returning to the previous slope tendency, while  $Kx$  has a more smooth transition to its peak of magnitude but afterwards goes to a bigger slope with its magnitude response declining more rapidly than  $Kq_1$ , Fig. 9.

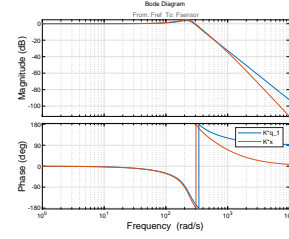


Fig. 9. Force Control: Comparison between the two outputs  $Kq_1$  and  $Kx$ .

**Sensitivity Analysis** A final sensitivity analysis is in order now with the complete cascaded loop control implemented.

**2.4.3.1. Mass** The natural frequency decreases as  $m$  increases. The behavior of  $Kq_1$  remains similar within the frequency range, but the  $Kx$  behavior changes dramatically for values above 1kg. Because the control variable used is  $q_1$ , the remaining degree of freedom  $x$  is free and its Bode Diagram is expected considering a mass  $m$  at the end of a spring.

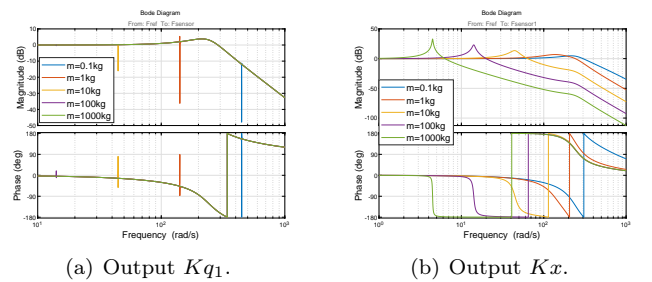


Fig. 10. Force Control - Mass Influence: Bode Diagram with input  $F_{ref}$ .

**2.4.3.2. Friction Coefficient** Looking at the influence of the friction coefficient, the behavior of  $Kq_1$  is almost identical except for the peak in magnitude that appears when  $f_{v2}$  is 0Ns/m. In terms of the behavior of  $Kx$ , up until a frequency of 100rad/s the behavior is unchanged but above this frequency the magnitude shows a departure from the initial dynamic response for  $f_{v2} = 0 \text{ Ns/m}$ , *i.e.* the magnitude's slope for higher frequencies decreases at

higher values of  $f_{v2}$ . In terms of phase,  $Kq_1$ 's behavior is almost unchanged except at the natural frequency. However  $Kx$ 's phase at higher frequencies, when increasing the viscous coefficient, will tend to zero, *i.e.* mass  $m$  will synchronize with mass  $M$ .

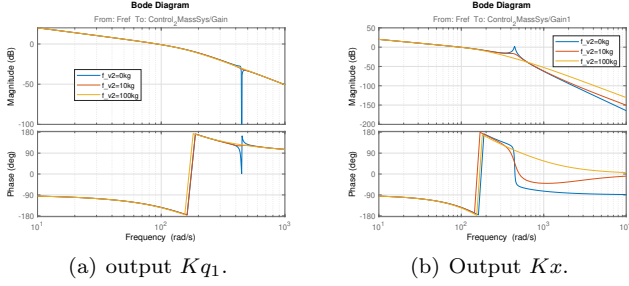


Fig. 11. Force Control - Friction Coefficient Influence: Bode Diagram.

### 3. VALIDATION OF SYSTEM OF TWO MASSES

#### 3.1 Introduction to dSpace

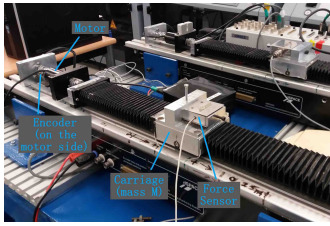


Fig. 12. dSpace - One Axis Robot.

The experiment environment is the dSpace shown in fig. 12, where we see the different practical elements with their correspondents to our model in analysis: 1) Carriage (mass  $M$ ); 2) Force Sensor (mass  $m$ ); 3) Motor (source of input  $F_m$ ); and 4) Encoder (velocity and position). During the experiments with dSpace an adjacent computer running the simulation is connected with dSpace, where we store the different sensor information. While using the velocity or the position of the carriage we must take care of which values refer to which reference, *i.e.* that the value from the encoder is measuring on the motor side and the controller's calculations are done in the carriage's side, *i.e.*  $q_{carriage} = Rq_{motor}$  with  $R=3.979 \cdot 10^{-4}$  m/rad.

The carriage's velocity and the force sensor's data are the main values used for control as explained before, the remaining sensor information such as the position and the current will be used to compare to the values obtained with the dynamic model designed in the previous chapter, to validate its information and confirm the veracity of the new parameters' values. Throughout the experiments different mass configurations were used.

#### 3.2 Model Validation

To begin the validation of the system, we start with an impulse response experiment, where we give an impulse to  $F_e^*$  and analyse the force sensor's response. In this experiment we want to guarantee that the response is only

due to the input of  $F_e^*$  and not  $F_m$ . If we acknowledge that the mass value of  $M$  is much higher than  $m$  and that the damping value of  $f_v$  is high enough, then an impulse of  $F_e^*$ , of small value, will not affect the dynamics of  $M$ . To make sure that this affirmation is true, experiments with the velocity controller of  $\dot{q}_1$  set at zero. In fig. 13 we see the impulse response in force for each of the three different mass configurations. For a higher mass value the natural frequency decreases Fu and Song (2019). These time values can be checked in table 2. Considering only

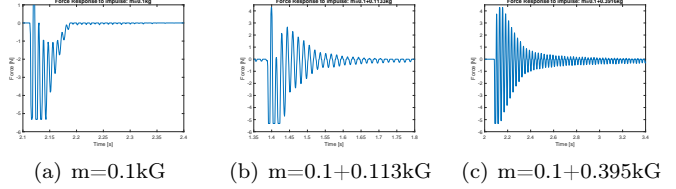


Fig. 13. Force Response to Impulse Input - Mass Configurations.

the force profile for the third mass configuration  $m = 0.1 + 0.395$ kG (which has a better and clearer result), the system has a sinusoidal response and an exponential decrease in magnitude. The latter observation is of interest because we can define an exponential function and calculate its time constant  $T$  to deduce the real friction coefficient value  $f_{v2} = 5.2585$ Ns/m.

Table 2. Force Impulse Response - Time values

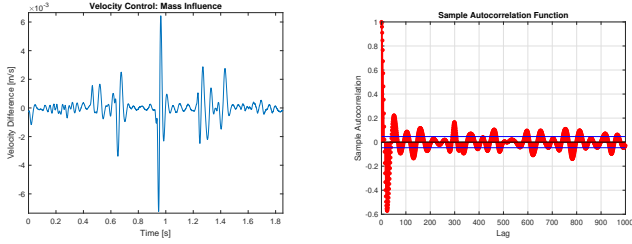
Mass $m$ [kG]	Simulation Frequency [rad/s]	dSpace Frequency [rad/s]	Percentage of Error [%]
0.1	448.8	698.1	35.7
0.1+0.1133	314.2	392.7	20.0
0.1+0.3916	202.7	251.3	19.3

#### 3.3 Velocity Control

Considering only the velocity control loop, to evaluate the accuracy of the simulation considering the dSpace experiments, first we calculate the difference between the simulation profile and the dSpace profile. Figure 14(a) shows the result of the velocity difference with root mean square value of  $10^{-3}$ m/s, and the peak value of difference happens during the step sequence at 1s. Afterwards, the autocorrelation function of the velocity difference was used to conclude if the model is able to reproduce the dynamic patterns that have been observed in the real system. Since the result from the autocorrelation function drops to zero very fast (in 72 lags), the velocity difference can be described as a random uncorrelated series of time, which also means that the simulation output and the reality's only difference is noise and not unmodeled dynamics. With this we conclude that the simulation's output is very close to the observed real output.

#### 3.4 Mass Influence

To see the evolution of the velocity response when increasing the mass  $m$  value, we consider three mass configurations:  $m = \{0.1, 0.1 + 0.1133, 0.1 + 0.3916\}$ kG. The difference in velocity profiles between the experiment and



(a) Velocity error between experiments and simulation. (b) Autocorrelation Function.

Fig. 14. Velocity Control with  $m = 0.1\text{kG}$ .

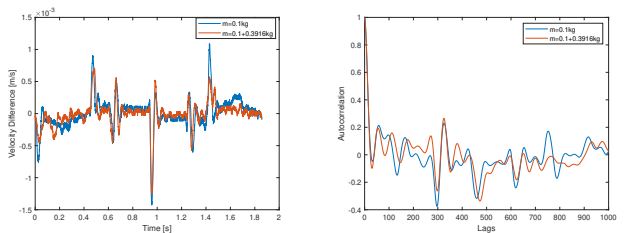
simulation and for different mass values the tendency is maintained. Afterwards, we do the same procedure now considering the autocorrelation functions seen in fig. 14(b). Even with a changing mass value, our autocorrelation function is practically the same, *i.e.* the velocity difference between simulation and observed real output is not influenced by mass  $m$  value.

In conclusion the different mass configurations the velocity controller is able to maintain the same performance (time response, transient response and steady state response); and the difference between the result from the model implemented and the result from the dSpace experiment is constant. The root mean square error of the velocity response with respect to the reference is maintained constant both for the simulation and the experiment.

### 3.5 Force Control

Considering the full control scheme dSpace is set up without any obstacles and a force trajectory is chosen as input reference  $F_{ref}$ .

**Trajectory** The velocity error is analyzed, with the two mass configurations  $m = \{0.1, 0.3956\}\text{kG}$ . Analyzing the



(a) Velocity error in m/s. (b) Autocorrelation Function of the Velocity Difference.

Fig. 15. Velocity error between experiments and simulation - Mass Influence.

velocity error profiles we obtain the root mean square value of 1.93% for a lower mass and a higher mass configuration has a value of 2.06%, whose values are very close to each other. Afterwards, the autocorrelation function is used with velocity error as input for each mass, obtaining the results seen in fig. 15(b), where we see the same tendency for both masses. As before, since the autocorrelation function quickly tends to zero, its time series is uncorrelated and is said to be a random signal, *i.e.* the simulation results are very close to the reality they are meant to represent.

## 4. CONCLUSIONS

A complete two mass model is defined with an interaction of the type spring-damper system, that simulates with accuracy an EMPS prototype. A cascaded loop control was implemented with an inner loop controlling the velocity  $\dot{q}_1$  and an outer loop controlling the interaction force between the two masses. In this new model, two new major variables were added: mass  $m$  and the viscous coefficient  $f_{v2}$ , to understand their influence in the overall model, a sensitivity analysis was done at three different stages: model writing, velocity control implementation and force control implementation. In terms of the mass  $m$ , its value of 0.1kG was of little significance when compared with the remaining dynamics within the system.

To follow the simulation work, a validation of the system was performed and an equivalence between the theoretical model and the real system was established, considering different mass  $m$  values. During the validation process a real value for the added variable  $f_{v2}$  was found.

## ACKNOWLEDGEMENTS

This work was supported by FCT, through IDMEC, under LAETA, project UIDB/50022/2020, and Cluster Fame Isit Next, Nantes University.

## REFERENCES

- Albu-Schaffer, A., Haddadin, S., Ott, C., Stemmer, A., Wimbock, T., and Hirzinger, G. (2007). The dlr lightweight robot : Design and control concepts for robots in human environments. *Industrial Robot-An Int. J.*, 34, 376–385.
- Albu-Schaffer, A. and Hirzinger, G. (2002). Cartesian impedance control techniques for torque controlled lightweight robots. In *Proc. 2002 IEEE Int. Conf. on Robotics and Automation (Cat. No.02CH37292)*, volume 1, 657–663.
- Albu-Schaffer, A., Ott, C., Frese, U., and Hirzinger, G. (2003). Cartesian impedance control of redundant robots: recent results with the dlr light weight arms. In *2003 IEEE Int. Conf. on Robotics and Automation (Cat. No.03CH37422)*, volume 3, 3704–3709.
- Devie, S., Robet, P., Aoustin, Y., and Gautier, M. (2018). Impedance control using a cascaded loop force control. *IEEE Robotics and Automation Letters*, 3(3), 1537–1543.
- Devie, S., Robet, P., Aoustin, Y., Gautier, M., Jubien, A., and Furet, B. (2017). Accurate force control and co-manipulation control using hybrid external command. *IFAC-PapersOnLine*, 50, 2235–2240.
- Fu, L. and Song, A. (2019). Model-based load characteristics analysis of the multi-dimensional force sensor. In *2019 19th Int. Conf. on Control, Automation and Systems (ICCAS)*, 1577–1582.
- Yi, N., Xiao-jun, G., Xiao-ru, L., Xiang-feng, X., and Wan-jun, M. (2010). The implementation of haptic interaction in virtual surgery. In *2010 Int. Conf. on Electrical and Control Engineering*, 2351–2354.
- Zhang, H., Li, B., Yuan, W., Kraft, M., and Chang, H. (2016). An acceleration sensing method based on the mode localization of weakly coupled resonators. *Journal of Microelectromechanical Systems*, 25(2), 286–296.